Macro–Micro Failure and Energy Evolution in Heterogeneous Fault Rock Masses

Yunjuan Chen · Mengyue Liu · Tao Gao · Yi Jing

Abstract XRD diffraction scanning tests were utilized to determine rock mineral composition, and a numerical calculation model of heterogeneous granite was established utilizing the PFC. The macro and micro damage characteristics of the heterogeneous granite model were analyzed. During failure, the boundary energy, strain energy, and dissipation energy were monitored. The results indicates that confining pressure can enhance the elastic modulus of the model by approximately 1.5 times. Under non-confining pressure conditions, shear failure is dominant in the model. Conversely, under confining pressure conditions, tensile-shear composite failure is prevalent. The micro-failure types are mainly slippage failure and shear failure. The microstructural strength of Albite and Quartz is found to increase with rising confining pressure, whereas that of Kaolinite is inhibited. Confining pressure has little effect on the microstructural strength of Potassium Feldspar. The critical confining pressure for the model is determined to be 15 MPa; strain energy is the dominant energy component at pressures below this threshold, while dissipation energy become dominant above it. At the micro-level, the boundary energy in the crack initiation energy is more sensitive to the confining pressure. In the peak strength energy, the growth rate of strain energy is greater than that of dissipation energy.

Y. Chen · M. Liu (✉)
School of Civil Engineering, Shandong Jianzhu University, Jinan 250101, Shandong, China
e-mail: liuyuximeng@163.com

Y. Chen
e-mail: skdcyj@126.com

Y. Chen
Key Laboratory of Building Structural Retrofitting and Underground Space Engineering, Ministry of Education, Shandong Jianzhu University, Jinan 250101, Shandong, China

T. Gao
Shandong Earthquake Agency, Jinan 250014, Shandong, China
e-mail: gaotaosju@126.com

Y. Jing
School of Qilu Transportation, Shandong University, Jinan 250002, Shandong, China
e-mail: jing1hay@163.com

1 Introduction

The construction of tunnel foundation engineering is growing, and the problem of complex underground space excavation is becoming more prominent. Especially in different geological structures, rocks have different macro–micro scale characteristics. The essential properties and mechanical characteristics

of rocks are often controlled by the micro-scale mineral structure, making it difficult to master the engineering surrounding rock structural properties and micro-structural. These factors are important reasons for rock fracture damage and engineering disasters (Wang et al. 2018; Zhu et al. 2019; Chen et al. 2020). Therefore, exploring the large-scale macroscopic damage caused by rock micro-damage and the energy evolution relationship during the damage (Gao et al. 2020; Reches and Wetzler 2022; Chen et al. 2022; Li et al. 2023) plays a crucial role in providing new ideas for revealing the intrinsic damage mechanisms in surrounding rock of different structural zones, and scientifically guiding engineering construction and mechanical disaster prevention.

External loads first drive changes in the mineral structure, and as the stiffness of the internal mineral particles gradually deteriorates, the original continuous medium characteristics of the mineral particles are lost, resulting in microstructure cracking of the rock and then cause the production of macroscopic cracks. However, there are significant differences in the internal microstructures and composition of different rocks, and these differences are the most important factors affecting the macroscopic mechanical properties of rocks (Lindqvist et al. 2007; Li et al. 2014). In response to differences in the microstructure of rocks, scholars at home and abroad have employed various research methods, including CT digital imaging (Chen et al. 2021; Feng et al. 2023), polarized microscopy analysis (Rubo et al. 2019), and XRD diffraction analysis (Chander et al. 2020). Hoagland (1973), Hallbauer (1973), Lindqvist (2007), and others used an optical microscope to observe the rock cracked by axial compression and found that different micro-mineral structures have a significant influence on macroscopic rupture. Jeong et al. (2017) studied the fracture toughness variation of granite from the microscale to the macroscale, and Alneasan et al. (2021) studied the influence of grain size and mineral composition on the propagation path and fracture speed of cracks, finding that fracture speed, fracture toughness, bending coefficient as well as the ratio of intergranular cracks and intragranular fractures is inversely proportional to the grain size. Yu et al. (2021) used uniaxial compression tests and numerical simulation methods to analyze the influences of the rock mineral particle size effect and spatial arrangement on the macroscopic mechanical behavior and

fracture, revealing that the cumulative and extended damage to individual mineral particles is the main factor causing macroscopic rock fracture. Li et al. (2021) conducted mineral composition, particle size, and hardness tests on 96 samples, and established a sample prediction function through raw test data and back-propagation artificial neural networks to study the relationship between mineral composition and inherent mechanics. Indoor experimental techniques cannot dynamically observe the microscopic structure's fracture damage in real time, and some researchers prefer numerical calculations to compare with experiments and find a theoretical model that can replace experiments. Daraei et al. (2023) studied the influence of micro-cracks on static elastic modulus and proposed a method to predict static elastic modulus by using the correlation between dynamic and static elastic modulus, which provided a reference for the determination of parameters in numerical simulation. Zheng (2023), Quan (2023), and others analyzed the micro-fracture characteristics and fracture mechanisms of granite based on the PFC3D-GBM model, verified the granite microcosmic numerical model's fracture mechanism during loading, and found that micro-damage is selective for certain minerals. They studied the impact of σ_2 and σ_3 on the microstructure's fracture in marble and predicted the pre-instability phenomenon of marble based on the microstructure's damage characteristics.

Microscopic structure accumulation damage in rock leads to macroscopic crack propagation and fracture. The essential attribute of macroscopic and microscopic rock damage is energy-driven evolution. Internal energy state of rock varies greatly with changes in stress state and mineral particle stability of the microscopic structure (Xie et al. 2008; Yu et al. 2020; Li et al. 2022). Huan (2017) considered the heterogeneity of rocks and proposed an energy evolution scale model for the microscopic damage of heterogeneous rocks by combining microscopic fracture mechanics, mathematical statistics theory, and energy damage evolution analysis. Chen et al. (2020) studied the effects of inclination angle and length on crack propagation behavior, failure mode, energy evolution and displacement distribution of surrounding rock by using the method of triaxial compression test and numerical simulation through parameter analysis. Zhang et al. (2019) studied the energy tendency problem of granite at the microscopic level using a

triaxial cyclic loading and unloading method. They established rock burst tendency evaluation indicators for different confining pressures from the microscopic energy perspective and revealed the energy evolution law of stress threshold values. Sun et al. (2020) used the PFC particle flow software as a basis to study the macroscopic and microscopic fracture characteristics and energy scale effect relationships of granite. When analyzing granite engineering problems, they found that the microscopic particle flow model has a certain scale effect. Chen et al. (2022) compared DDARF and RFPA software to study the microscopic fracture extension and energy evolution damage of jointed rock masses and obtained that microscopic damage presents the trend of stable growth—rapid growth—stable growth in jointed rock masses. Yingquan et al. (2022) simulated the microscopic cracking process of minerals under unloading conditions using particle flow software and summarized the law of energy trend under different crack penetration patterns to provide simulation references for the microscopic mechanical mechanism of crack penetration and energy damage of rock cracking.

Currently, how to study the fracture mechanism of microscopic mineral rocks better and how to combine microscopic damage with the essence of energy damage remains the main problem. Therefore, based on indoor experiments and numerical simulation, this article used X-ray diffraction analysis technology to obtain the microscopic mineral composition of the engineering granite and optimized the numerical calculation model of the discrete element particle flow to investigate the macroscopic and microscopic mechanical characteristics of the heterogeneous granite model under different confining pressures. The changes in strain energy, dissipation energy, and boundary energy under microscopic damage were analyzed. Aiming to provide specific references for conducting damage and fracture analysis of surrounding rocks in underground engineering, and for rock as well as soil engineering design from multiple analysis scales.

2 Engineering Background and Indoor Testing

2.1 Engineering Rock Mass Characteristics

Selecting a deep-buried ultra-long tunnel engineering project, the tunnel geological zone is located in the middle of the high mountain area of southwestern Sichuan. The overall terrain is undulating, with elevations mostly around 850–2500 m. The surrounding rock of the tunnel is mainly moderately weathered granite, which is determined to be relatively hard on-site and presents a block-like structure with well-developed joints and fissures. The tunnel design length is 7286 m, with a maximum depth of 1270 m. The main tunnel has a vault height of 7.15 m and a distance of 11.06 m between the left and right sidewalls. It passes through multiple fault zones, of which the surrounding rock in fault zones of grade V and IV accounts for about 33% of the total length, while other surrounding rock is of grade III conventional rock. Overall, this tunnel is considered a high-risk ultra-long and deep-buried geological tunnel. The tunnel longitudinal section layout diagram is shown in Fig. 1. Based on this understanding and to ensure absolute safety during construction, a mechanical failure analysis is carried out on this tunnel to properly understand the failure mechanism of the surrounding rock.

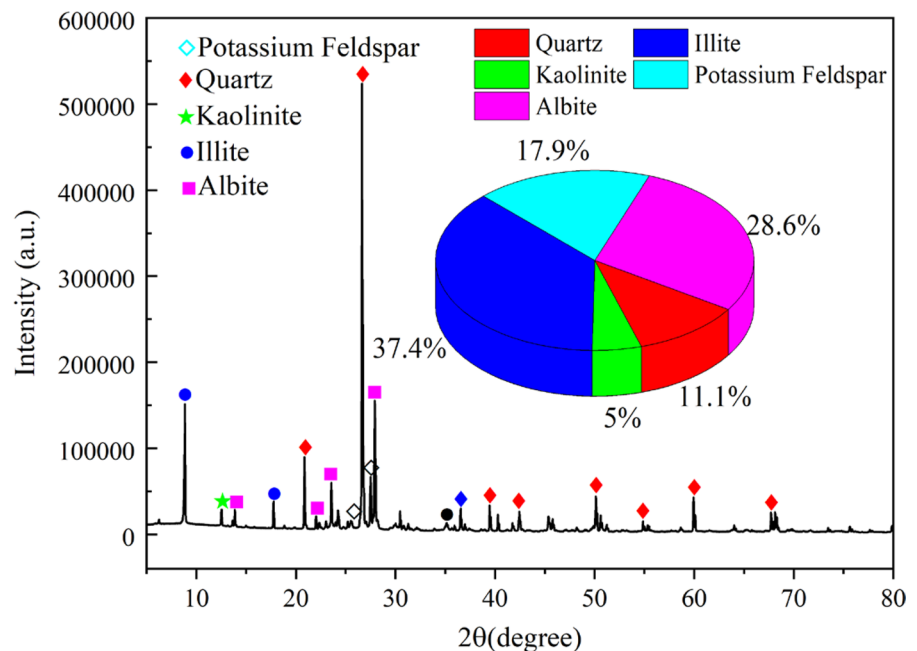Fig. 1 Tunnel longitudinal section layout diagram
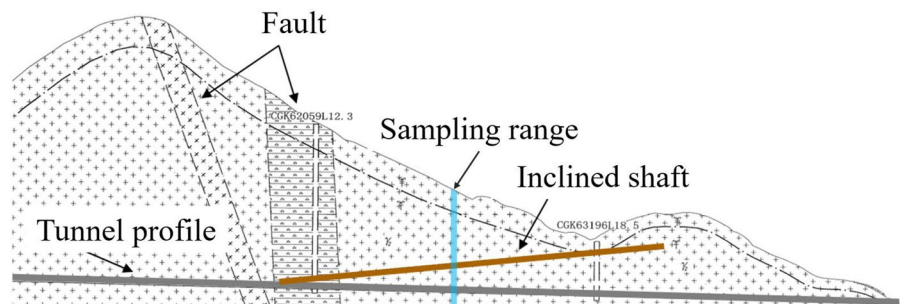
2.2 X-ray Diffraction Test Analysis

In order to reveal the relationship between the fracture mechanism of deep-seated surrounding rock and the micro mineral structure, indoor tests were adopted as a basic research method, X-ray diffraction (XRD) tests on granite were conducted. The specimens were taken from the class III surrounding rock section of Lushi Tunnel, the parameters of rock are shown in Table 1. The specimens are processed in strict accordance with the requirements of International Society of Mechanics (ISRM) and Standard for Test Methods of Engineering Rock Mass (GB/T 50266-2013). The size of the specimens after processing is 50 mm in diameter and 100 mm in height. After processing, some samples were sampled and ground for XRD testing. The range of X-ray diffraction angle 2θ is $0\sim80°$, qualitative and quantitative phase analysis method was used. The element qualification method was used to search for mineral elements present in the
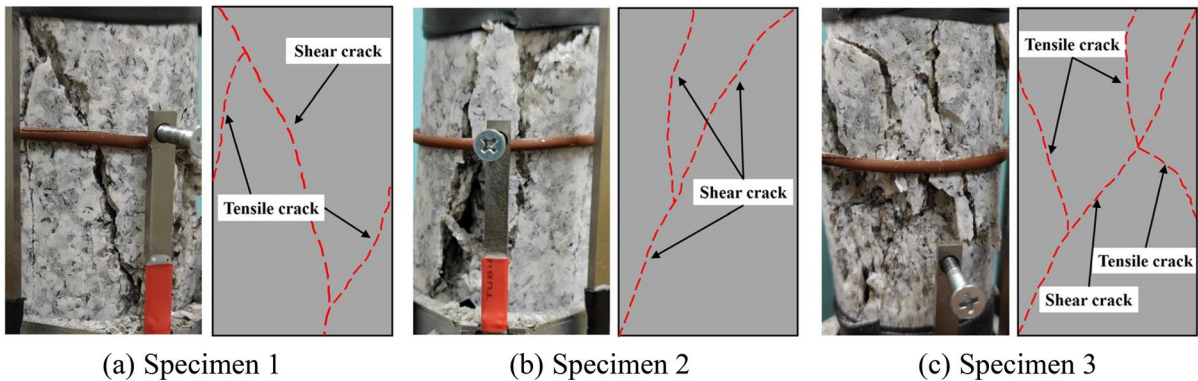
sample, and the specific results of the mineral composition of the surrounding rock were finally determined as shown in Fig. 2.

It can be seen from Fig. 2 that the mineral component with the highest content in the surrounding rock is Illite, with a content of 37.4%, Albite and Potassium Feldspar with 28.6% and 17.9% respectively, Quartz with 11.1%, and Kaolinite with the lowest content, only about 5%.

2.3 Axial Compression Test Analysis

The TAW-1000D rock rheological disturbance tester was used to perform mechanical performance tests, with a maximum axial compression load of 1000 kN and a loading rate of 0.1 mm/min for each rock sample. The failure modes of each specimen are shown in Fig. 3.

As can be seen from Fig. 3, the rocks mainly failed in shear, with shear cracks continuously penetrating and forming the main rupture surface under the action of axial compression load. The cracks gradually extend to the upper and lower end surfaces of the specimen. During the process of the main rupture surface penetration, influenced by local tensile stress, resulting in secondary tensile cracks parallel to the axial direction. The angle between the tensile crack and the main rupture surface is mostly less than 90°,

Table 1 Main Parameters of Surrounding Rock

Rock classification	Density ρ(g/cm^3)	Elastic modulus E (GPa)	Poisson ratio v	Cohesion c (MPa)
III	2.68	57.8	0.25	19.6

Fig. 2 XRD spectrum and mineral composition of samples

(a) Specimen 1   (b) Specimen 2   (c) Specimen 3

Fig. 3 Macroscopic morphology of specimen failure

indicating that the initiation of local tensile cracks is mainly controlled by the influence of shear action, which is a secondary crack in the development of shear cracks. During loading, indications of rockburst manifested with a "loud noise", causing the surface of the specimen to peel off and disintegrate. This suggests that the primary factor is the joint action of tensile cracks extending to the specimen's surface and radial tensile stress. This combination promotes crack propagation through the local surface, ultimately resulting in the formation of a free body.

At the same time, the mechanical parameters and failure modes of each group of specimens in Fig. 3 are extracted to provide basic mechanical parameters and verification analysis for the numerical model.

3 Heterogeneity Granite Discrete Element Numerical Simulation

3.1 Numerical Model Establishment

Rocks are composed of different mineral particles arranged in a heterogeneous manner, and the heterogeneous distribution of these particles is the fundamental cause of rock cracking. Therefore, based on X-ray diffraction analysis, a heterogeneity discrete element numerical calculation model of granite is established. PFC2D is used to establish the numerical model, by conducting reductive simulation of five mineral particles and writing FISH functions, a two-dimensional numerical model of granite is generated, with a total of 11,606 particles. The parallel bonding model is used to better simulate the bonding and crack propagation behavior in granular materials such as rocks. The bottom boundary of the model is a fixed wall, the top boundary is usually a wall that can move in a vertical direction, a constant speed or pressure can be applied from the top to simulate uniaxial compression, the side boundary is a free boundary, and some boundary particles can be placed near the wall to better simulate the interaction between the wall and the particle. The size of the model is the same as that of the specimen, with a diameter of 50 mm and a height of 100 mm, numerical model as shown in Fig. 4.

Figure 4 shows different methods of generating particles for heterogeneous granite models. It can be seen that the dispersibility of each type of mineral particles in the traditional heterogeneity model is relatively large, while the minerals in the actual rock structure have a certain agglomeration characteristic. Moreover, the microscopic distribution of traditional model particles has the characteristics of point-like and striped, as shown in Fig. 4d, which is not consistent with the conventional microscopic features of rocks. Therefore, the FISH language is optimized, through introducing the Weibull distribution function (math. random. uniform) encoding processing to obtain random numbers between 0 and 1, then the flexible cluster is used to globally traverse all particles to ensure that the particle distribution shape is more consistent with the conventional microscopic morphology of rocks.
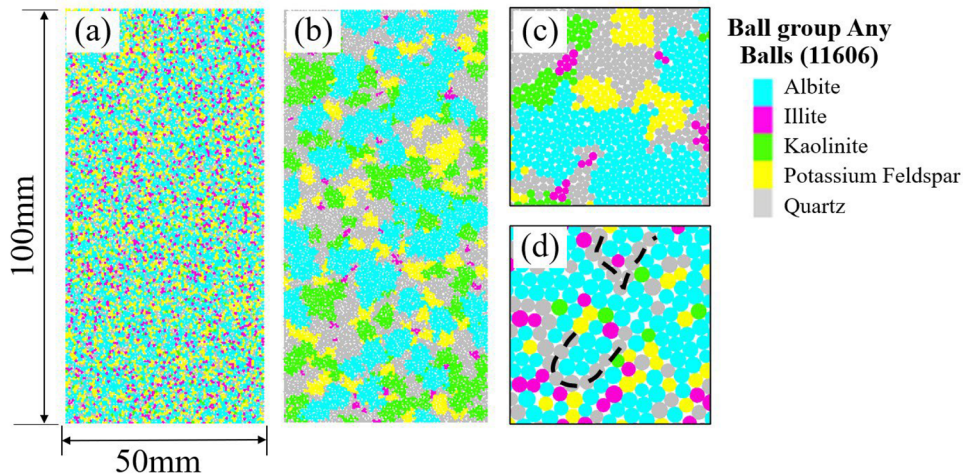
(a)Conventional Model, (b)Optimal Model, (c) Conventional Microscopic view, (d) Optimal Microscopic View

Fig. 4 Heterogeneity granite numerical model:

3.2 Microscopic Parameter Verification

Reasonably determining the mechanical parameters of rocks is the key to numerical simulation. In order to make the mechanical properties of the numerical model consistent with the physical model experiment, it is necessary to determine the microscopic parameters of the model. The PFC program characterizes the overall force and displacement of the model through micro-level contact. The preset physical quantities of particles and contacts are only at the micro-level, and have no direct correlation with the macroscopic mechanical properties of the model. Therefore, the parameter range is preliminarily established by consulting the case of various mineral parameters in rock mechanics, and then it is necessary to conduct a lot of trial and error with preset parameters (Li et al. 2022), compare with indoor physical tests, and constantly correct parameters, and finally obtain the parameter set required for this numerical simulation. The stress–strain curve of the final numerical model is extracted and compared with indoor experiment, verification result as shown in Fig. 5. From the macroscopic failure morphology and curve trend, the heterogeneous granite numerical model and the indoor experimental results are well matched, and the peak strength is basically the same, indicating that the numerical model parameters are accurate and

reasonable. This parameter is used as the basis for subsequent research, and the specific parameters are shown in Table 2.

## 4 Analysis of Macro–Micro Characteristics of Heterogeneous Granite Damage

The mechanical behavior of the surrounding rock in ultra-long and deeply buried tunnels is complex, and the disturbance of the surrounding rock varies greatly at different depths and with different construction schemes. Studying the destruction of different mineral particles under uniaxial compression tests has certain limitations. However, by applying different confining pressure loads, the multi-scale destruction characteristics of engineering surrounding rock under different stress environments can be well reflected. Therefore, by applying multiple confining pressure conditions of 0, 5, 10, 15, 20, and 30 MPa to the numerical model of heterogeneous granite, the mechanical characteristics of heterogeneous granite are analyzed.

4.1 Analysis of Stress–Strain Curve and Macroscopic Crack Extension Pattern

Figure 6 shows the stress relationship and crack situation of the heterogeneous granite model under
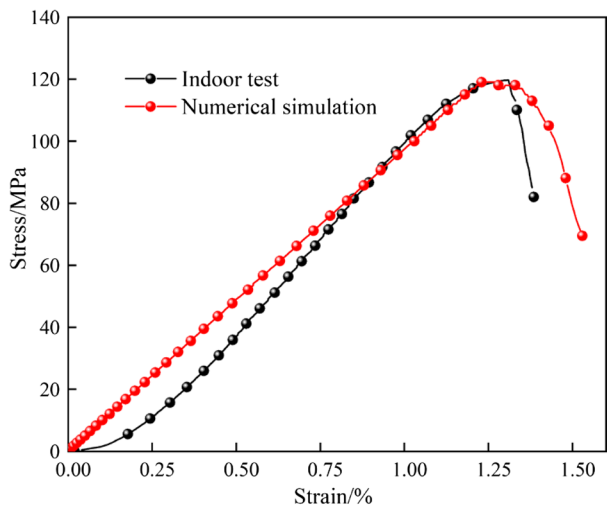
(a) Stress-Strain Curve Relationship
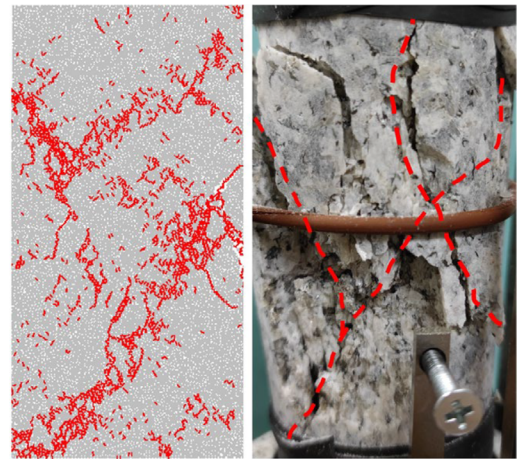
(b) Comparison of Macroscopic Rupture of Specimens

Fig. 5 Comparison of indoor test and numerical simulation results

Table 2 Main Parameters of Inhomogeneous Granite Model

Mineral name	Density ρ(g/cm^3)	Effective elastic Modulus E_c(GPa)	Stiffness ratio k_n/k_s	Friction coefficient μ	Porosity λ	Strength of extension σ_c(MPa)	Cohesion c(MPa)
Quartz	2.80	60	2.5	0.51	3.5e-5	265	280
Potassium Feldspar	2.70	45	2.5	0.50	3.1e-5	130	135
Albite	2.65	42	2.5	0.46	2.9e-5	110	120
Illite	2.70	11	2.5	0.50	2.4e-5	30	150
Kaolinite	2.75	18	2.5	0.50	3.4e-5	25	140

different confining pressures. As shown in Fig. 6a, the static elastic modulus (Hereafter it is referred to as elastic modulus.) of the specimen is significantly affected by the confining pressure, and the confining pressure conditions increase the elastic modulus by nearly 1.5 times. This indicates that the confining factors can increase the elastic modulus of the rock and make the rock more prone to strain softening characteristics. The strain under the 30 MPa high confining pressure is much larger than that under the smaller confining pressure conditions, indicating that under the high confining pressure, external disturbances are more likely to cause significant deformation of the surrounding rock. During the post-peak stress drop stage, the stress paths under different confining pressure conditions are similar, which also explains that the macroscopic crack rupture shape has a certain similarity (see Fig. 7). As shown in Fig. 6b, the confining pressure conditions increase the peak strength by at least 2 times, and the peak strength increases proportionally with the enhancement of confining pressure. Under the condition without confining pressure, the number of tensile cracks is greater than that of shear cracks, but under the confining pressure conditions, the number of shear cracks is higher than that of tensile cracks. As the confining pressure increases, the difference between the two gradually increases, indicating that the destruction between the particles is mainly shear destruction, and tensile destruction is auxiliary.
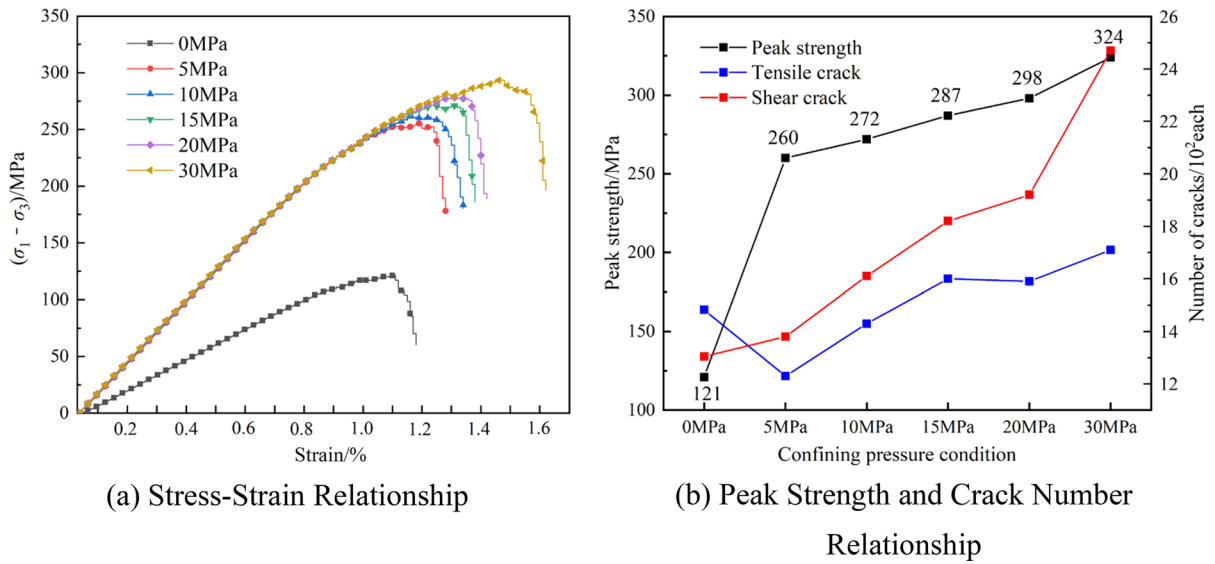
(a) Stress-Strain Relationship

(b) Peak Strength and Crack Number
Relationship

Fig. 6 Stress–Strain curve relationship and crack number under different confining pressures

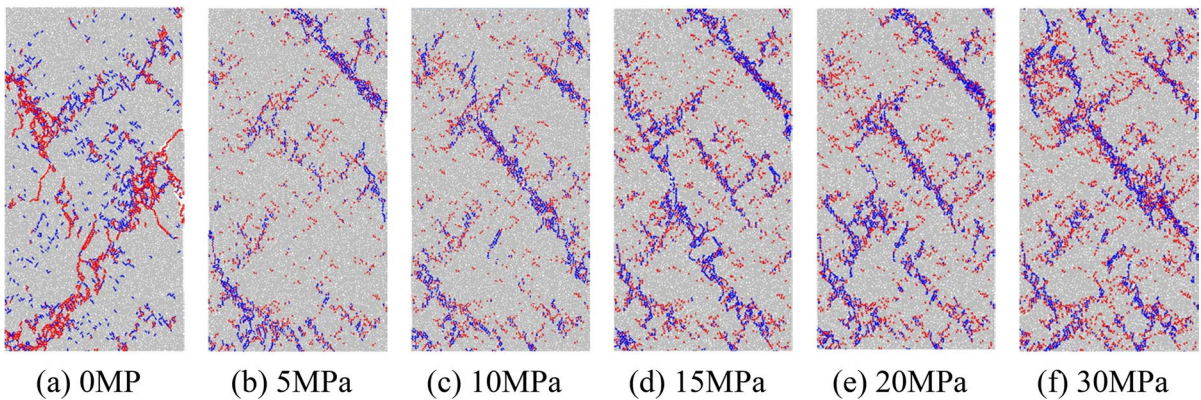(a) 0MP   (b) 5MPa   (c) 10MPa   (d) 15MPa   (e) 20MPa   (f) 30MPa

Fig. 7 Macroscopic fracture morphology of heterogeneous granite calculation model

Figure 7 shows the final fracture morphology of the numerical model of heterogeneous granite under confining pressures of 0–30 MPa. Red represents shear cracks, and blue represents tensile cracks. As shown in the figure, under uniaxial compression (0 MPa) loading, the specimen is mainly destroyed by shear, and as the axial load increases, more secondary tensile cracks are generated near the shear crack, which forms the main rupture surface influenced by the shear stress and extends to both sides of the specimen, causing instability and failure of the specimen. With the application of confining pressure loads, the specimen is mainly destroyed by tensile-shear composite type. Under relatively low confining pressure conditions (5 MPa, 10 MPa), the number of tensile and shear cracks is small, and the extension path of tensile cracks is basically parallel. The shear crack is generated near the tensile crack, and the positions of the two are approximately perpendicular to each other. Under the condition of high confining pressure (greater than 15 MPa), the crack density increases significantly, forming the main fracture path of multiple tensile cracks, and the main cracks are in a parallel relationship. When tensile cracks and shear

cracks converge, it is often the aggregation zone of rock fracture zone, indicating that the higher the confining pressure, the wider the rock failure range and the greater the rock fracture degree. These degrees of fragmentation are also the dominant factors leading to the increase of strain, which better verifies that rock disturbance under high confining pressure is easy to form large deformation hazards.

4.2 Cross-Scale Analysis of Macro–Micro Failure

Figure 8 shows the micro-damage morphology of different mineral particles, where the red line segment represents the shear crack and the blue line segment represents the tensile crack. The "tree-like" distribution of connections between particles represents the force chain structure of the model. Of which the force chain damage structure of the main minerals, including Potassium Feldspar, Albite, Kaolinite, and Quartz, was extracted.

Based on the figure, it can be seen that the tensile cracks are mainly concentrated near the Albite minerals, gradually extending to the interior of the Kaolinite, Potassium Feldspar, and Quartz minerals as the Albite minerals crack. Under uniaxial conditions, the internal microstructures of Albite and Quartz are mainly destroyed by sliding along the mineral particles, while those of Potassium Feldspar and kaolin are mainly destroyed by shearing through the mineral particles. When slippage destruction along the mineral particles occurs, the internal force chain structure is relatively small, whereas shear failure through minerals particles occurs, the force chain structure is relatively large and thick.

When confining pressure is applied, the force chain between the Albite mineral particles is relatively dense and large, and the microscopic destruction is mainly the shear failure through minerals particles. Confining pressure to some extent strengthens the microscopic force chain structure of Albite. When the confining pressure is between 0 and 5 MPa, the microscopic destruction of Kaolinite is mainly shear failure through minerals particles, and the force chain structure is relatively dense. After 10 MPa, the force chain structure becomes looser, and the microscopic destruction is mainly slippage destruction along the mineral particles. Indicating that confining pressure weakens the bonding between Kaolinite minerals, thereby reducing the strength of mineral particles. The force chain structure of Potassium Feldspar remains stable under varying confining pressures, with microscopic structural damage primarily is mainly shear failure through the mineral particles. The impact of confining pressure on Potassium Feldspar minerals can be considered negligible. When the confining pressure ranges from 0 to 10 MPa, microscopic damage to Quartz mineral particles manifests primarily through sliding along the mineral particles.

However, when the confining pressure increases, the Quartz mineral particles do not undergo destruction, and the force chain structure is relatively dense and uniform, indicating that the influence of confining pressure on enhancing the strength of the Quartz mineral is relatively stable. In summary, the mineral particles whose microscopic structural strength is enhanced with the increase of confining pressure are: Albite and Quartz; the microscopic strength of Kaolinite is inhibited as the confining pressure increases, and the influence of confining pressure on the microscopic strength of Potassium Feldspar is relatively small.

5 Heterogeneity Numerical Model Energy Damage Evolution Analysis

5.1 Principle of Heterogeneity Model Energy Calculation

The essential attribute of microscopic rock damage is the energy-driven evolution. Analyzing the relationship between energy during damage is important for understanding the rules of mineral particle damage, crack extension and rupture form, and macroscopic stability loss. Therefore, microscopic mineral damage and energy evolution in rocks are directly related.

Assuming the calculation model is in a closed state (i.e., no energy exchange occurs with the external environment), the energy relationship generated by the work during rock loading can be obtained, the total input energy U of the rock mass unit can be expressed from the first law of thermodynamics as Eq. (1).

$$U = U_d + U_e \qquad (1)$$

(a) 0MP

(b) 5MPa

(c) 10MPa

(d) 15MPa

(e) 20MPa

(f) 30MPa
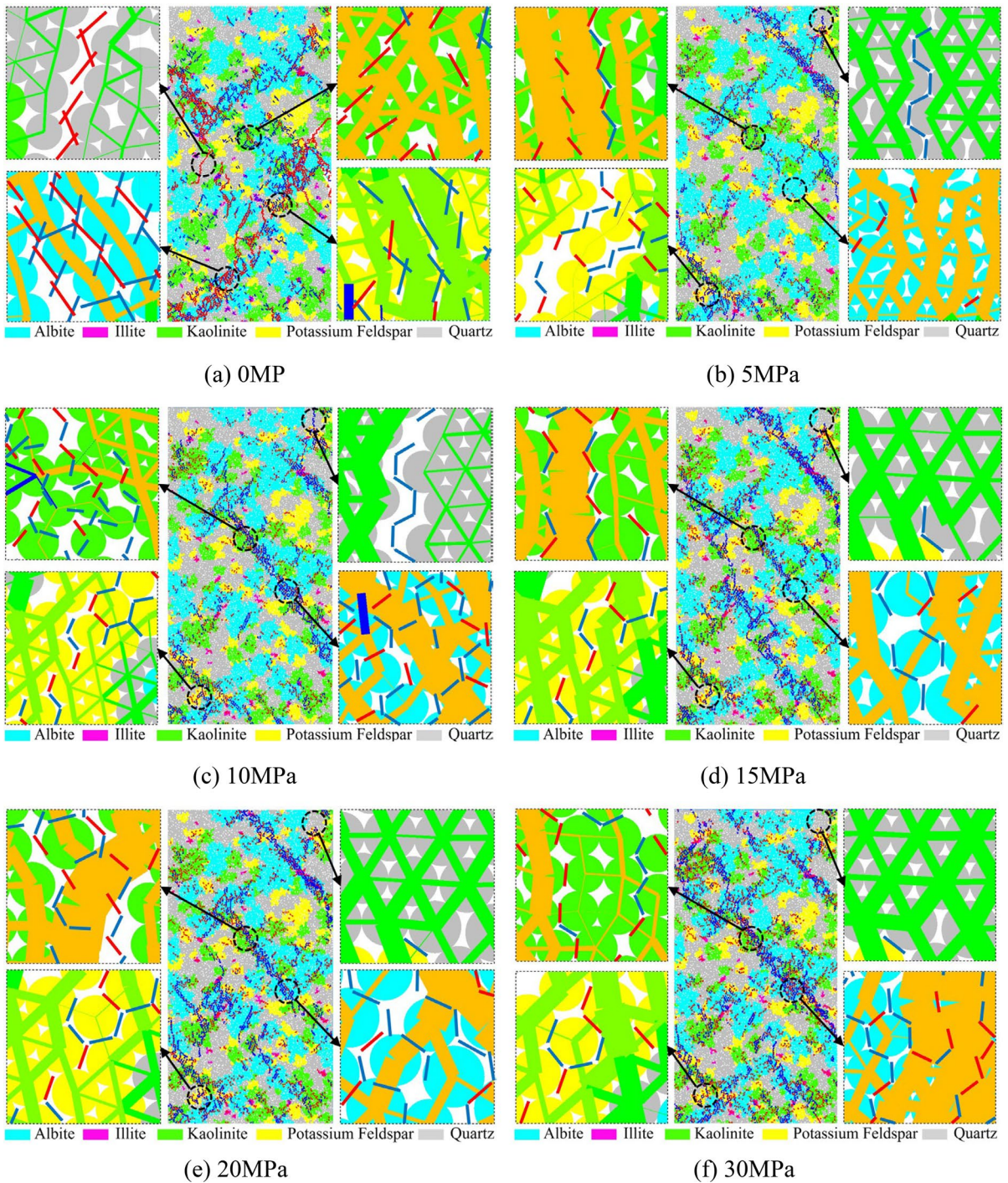
Fig. 8 Microscopic mineral fracture morphology of inhomogeneous granite

In the equation, U_d is the dissipation energy of the unit, mainly used for the internal crack friction damage and plastic deformation of the rock under external loading; U_e is the strain energy of the unit, mainly storing the elastic deformation of the rock in deformation and failure.

In the heterogeneity calculation model, the "set energy on" command is used to track and record the energy between particles. By loading the wall, the servo parameters can be set, and the boundary energy of the system, that is the total energy, can be obtained as Eq. (2).

$$U = U_{\text{ago}} + \left(F_1 \Delta S_1 + F_2 \Delta S_2 \right) \tag{2}$$

In the equation, U_{ago} is the total energy input into the system at the end of the previous calculation step; F_1 and F_2 are the magnitudes of the loading forces generated by the two loading walls for the current calculation step at unit displacement; ΔS_1 and ΔS_2 are the absolute value of displacement variation of the loading walls for the current calculation step.

The strain energy of particles in the linear parallel bond model is expressed as the sum of the parallel bond strain energy E_{k1} (represented by the "epbstrain" command in PFC) and the linear strain energy E_{k2} (represented by the "estrain" command in PFC), which can be expressed as Eqs. (3), (4) and (5).

$$U_{\text{e}} = E_{\text{k1}} + E_{\text{k2}} \tag{3}$$

$$E_{\text{k1}} = \frac{1}{2} \left(\frac{\overline{F}_{\text{n}}^{\,2}}{\overline{k}_{\text{n}}\,\overline{A}} + \frac{\|\overline{F}_{\text{s}}\|^2}{\overline{k}_{\text{s}}\,\overline{A}} + \frac{\overline{M}_{\text{t}}^{\,2}}{\overline{k}_{\text{s}}\,\overline{J}} + \frac{\|\overline{M}_{\text{b}}\|^2}{\overline{k}_{\text{n}}\,\overline{I}} \right) \tag{4}$$

$$E_{\text{k2}} = \frac{\|\overline{F}_{\text{s}}\|^2}{\overline{k}_{\text{s}}} + \frac{\|\overline{F}_{\text{n}}\|^2}{\overline{k}_{\text{n}}} \tag{5}$$

In the equation, $\overline{F}_{\text{n}}$ is the normal force of the parallel bond, $\overline{F}_{\text{s}}$ is the tangential force of the parallel bond, $\overline{M}_{\text{t}}$ is the torque, $\overline{M}_{\text{b}}$ is the bending moment, $\overline{k}_{\text{n}}$ is the normal stiffness of the parallel bond, $\overline{k}_{\text{s}}$ is the tangential stiffness of the parallel bond, $\overline{A}$ is the cross-sectional area of the contact surface, and $\overline{I}$ is the moment of inertia of the parallel bond section.

5.2 Analysis of Energy Evolution Process

Figure 9 shows the micro-energy evolution characteristics of the heterogeneity granite model under different confining pressures. It can be seen from Fig. 9 that the energy evolution basically presents a "slow growth-steady growth-fall" process. Dissipation energy is the main representational energy driving rock failure, the growth of which is proportional to the increase of the number of cracks under the no confining pressure condition, and the growth rate of crack growth in the later stage is greater than that under the confining pressure condition. After applying the confining pressure, the dissipation energy shows an energy drop phenomenon at the end of the growth stage and the rate of drop slows down, indicating that the confining pressure has a certain inhibitory effect on the extension of rock cracks. The change trend of strain energy is basically the same during the slow growth and steady growth stages, and during the energy drop stage, the strain energy drop rate is relatively slow under no confining pressure condition, but its drop rate increases significantly with the increase of confining pressure, indicating that the release rate of strain energy after the peak strength is controlled by confining pressure. The trend of boundary energy evolution is basically similar to that of strain energy, and with the increase of confining pressure, the difference between boundary energy and dissipation energy also increases proportionally, indicating that the total energy of the system is positively correlated with the confining pressure.

The microstructure damage of mineral particles under different confining pressures exhibits significant differences. In order to further investigate the energy characteristics of heterogeneous granite at different stages, microcosmic initiation energy of the crack and peak strength energy of stress were compared. Figure 10 shows the energy changes extracted at each characteristic point.

Based on the graph, it can be seen that both the energy required to initiate crack propagation and the peak stress intensity factor exhibit linear growth functions. Each energy index is within a 95% confidence interval of the theoretical predicted value, and the predicted precision of the relationship between energy index and confining pressure is high. The linear fitting of the energy curve increases as the stress reaches the peak intensity. When the confining pressure is less than 15 MPa, the strain energy required to initiate crack damage is higher than the dissipation energy, and the strain energy dominates. When the confining pressure is greater than 15 MPa, crack propagation requires more energy consumption, and the dissipation energy dominates. Therefore, the 15–20 MPa range is used as the boundary confining

(a) 0MP

(b) 5MPa

(c) 10MPa

(d) 15MPa

(e) 20MPa

(f) 30MPa
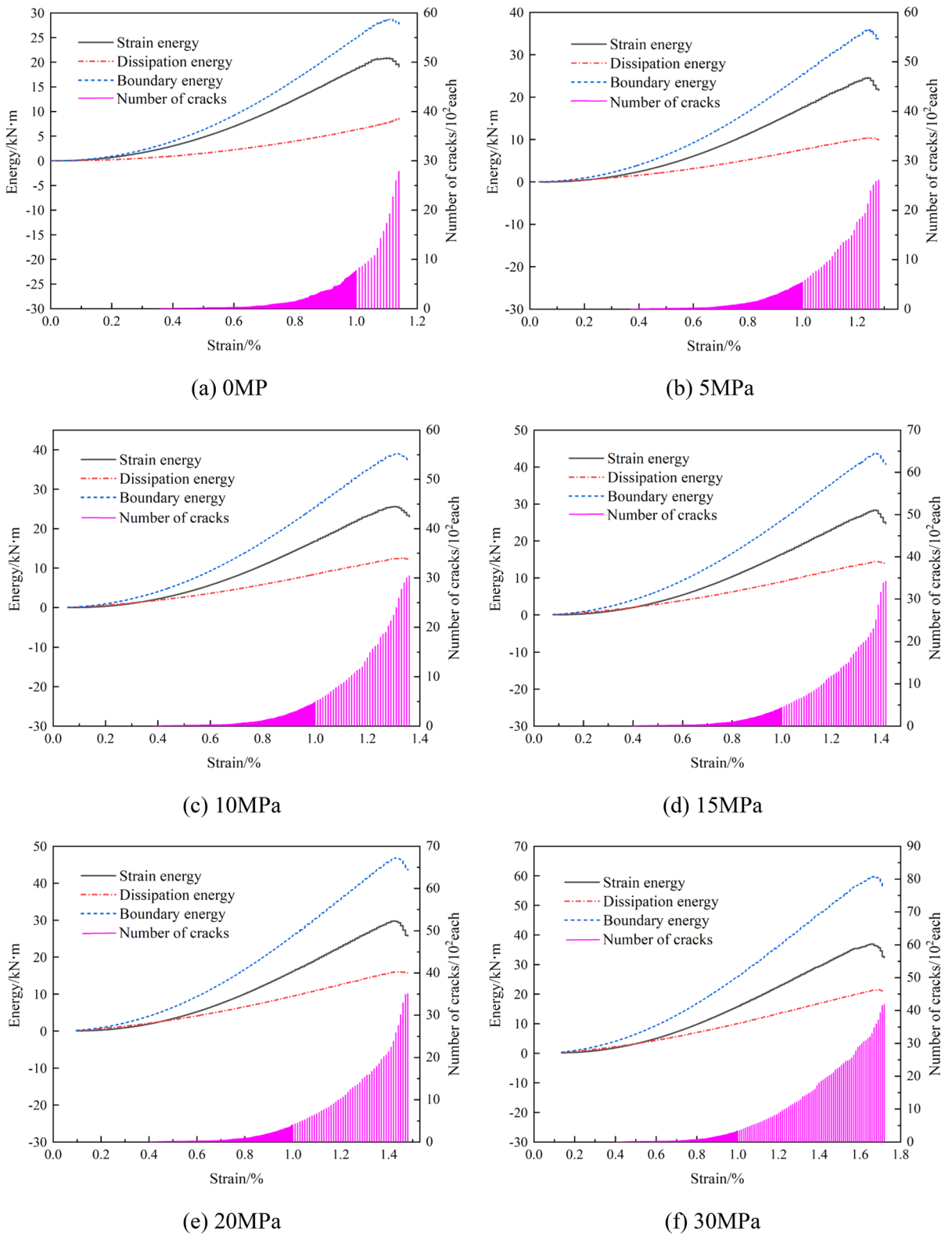
Fig. 9 Energy evolution curves under different confining pressures
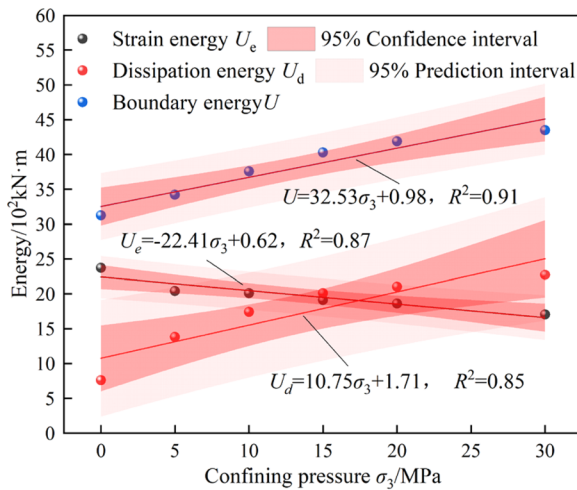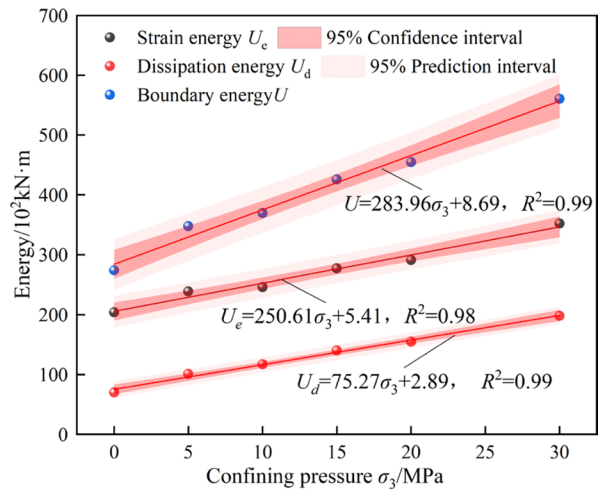
(a) Microcosmic Initiation Energy of the Crack　　　(b) Peak Strength Energy of Stress

Fig. 10 Characteristic energy under different confining pressures

pressure for rock strength classification. From Fig. 10a, it can be seen that when low confining pressure rocks crack, the microcracks are controlled by the elastic release of strain energy, and strain energy is the first dominant energy. When the confining pressure exceeds the boundary, the microcracks are controlled by the damage release of dissipation energy, and dissipation energy is the first dominant energy. This indicates that the microcracks mechanism which is dominant by the dissipation energy under high confining pressure conditions are more damaging, this kind of crack is irreversible damage compared with the crack caused by strain energy. From Fig. 10b, it can be seen that as the confining pressure increases, the strain energy, dissipation energy, and boundary energy all exhibit linear growth. The growth rate of strain energy is greater than that of dissipation energy, indicating that the specimen accumulated a large amount of strain energy at the time of peak failure. Under high confining pressure conditions, it is more favorable to store residual strain energy after the peak failure, which easily leads to unstable expansion and failure of post-peak cracks in rocks.

6 Conclusion

In order to study the macroscopic and microscopic failure types and energy evolution characteristics of granite, axial compression tests and mineral identification tests were carried out on granite, and a numerical model of heterogeneous granite was established. The following conclusions were drawn:

(1) Confining pressure increases the elastic modulus of heterogeneous granite by nearly 1.5 times. Under the 0 MPa condition, shear failure is the main type of failure, and under the increasing confining pressure, tensile-shear composite failure becomes dominant. The tensile crack propagation path is basically parallel, and shear cracks are generated near the tensile cracks. Under high confining pressure, the number of cracks increases significantly, forming multiple tensile main crack rupture paths.

(2) Under the 0 MPa condition, the microscopic failure of Albite and Quartz is slippage failure along mineral particles, while that of Potassium Feldspar and Kaolinite is mainly shearing fracture through mineral particles. Under confining pressure conditions, the microscopic failure of Albite, Potassium Feldspar and Quartz are shear fracture through mineral particles, while that of Kaolinite is mainly slippage failure along mineral particles. The strength of Albite and Quartz microscopic structures increases with rising confining pressure, whereas that of Kaolinite diminishes under elevated confining pressure. The influence of

confining pressure on the microscopic strength of Potassium Feldspar is relatively small.

(3) The whole microscopic energy evolution process of the heterogeneous model shows "slow growth-stable growth-fall". Confining pressure suppresses the later growth of dissipation energy. With increasing confining pressure, the rate of strain energy decline increases and the release rate has a more significant impact. The difference between boundary energy and dissipation energy increases proportionally with the increase of confining pressure.

(4) Taking 15 MPa as the boundary pressure between high and low limits of rocks, the microscopic crack initiation strain energy dominates when the pressure is less than 15 MPa, while dissipation energy dominates when the pressure is greater than 15 MPa. Boundary energy is more sensitive to confining pressure in the crack initiation energy. The strain energy, dissipation energy, and boundary energy in peak strength energy all show linear growth, and the growth rate of strain energy is greater than that of dissipation energy, which easily leads to unstable expansion and failure of post-peak cracks in rocks.

Data Availability   Not applicable.

Declarations

Conflict of interest   The authors declare that there are no conflicts of interest regarding the publication of this paper.

References

Alneasan M, Behnia M (2021) An Experimental investigation on tensile fracturing of brittle rocks by considering the effect of grain size and mineralogical composition. Int J Rock Mech Min Sci 137:1–14. https://doi.org/10.1016/j.ijrmms.2020.104570

Chander V, Tewari D, Negi V, Singhc R, Upadhyaya K, Aleya L (2020) Structural characterization of Himalayan black rock salt by SEM, XRD and in-vitro antioxidant activity. Sci Total Environ 748:1–10. https://doi.org/10.1016/j.scitotenv.2020.141269

Chen X-s, Xu Z-h, Bao X-h, Wang X-t, Fu Y-b (2020) Challenges and technological breakthroughs in tunnel construction in China. China J Highw Transp 33(12):1–14. https://doi.org/10.19721/j.cnki.1001-7372.2020.12.001

Chen S, Feng F, Wang Y, Li D, Jiang N (2020) Tunnel failure in hard rock with multiple weak planes due to excavation unloading of in-situ stress. J Cent South Univ 27:2864–2882. https://doi.org/10.1007/s11771-020-4515-7

Chen J, Zhang Z, Xu W, Li L (2021) Quantitative method of shape parameters of mineral particles based on image processing. J Eng Geol 29(1):59–68. https://doi.org/10.13544/j.cnki.jeg.2021-0003

Chen Y, Gao T, Gao C, Yin Y, Li Y (2022) Fracture propagation and acoustic emission energy damage law of fractured rock mass under hydraulic coupling action. J Cent South Univ Technol 53(6):2325–2335. https://doi.org/10.11817/j.issn.1672-7207.2022.06.032

Chen YJ, Gao T, Yin FQ, Liu XZ, Wang J (2022) Study on influence of joint locations and hydraulic coupling actions on rock masses' failure process. Energies 15(11):1–14. https://doi.org/10.3390/en15114024

Daraei A, Sharifi F, Qader DN, Hama Ali HF, Kolivand F (2023) Prediction of the static elastic modulus of limestone using downhole seismic test in Asmari formation. Acta Geophys. https://doi.org/10.1007/s11600-023-01109-1

Feng Q, Hou SJ, Liu WW, Zhang S, Li WS, Tian ML (2023) Study on the simulation method and mesoscopic characteristics of rock freeze-thaw damage. Comput Geotech 153:1–22. https://doi.org/10.1016/j.compgeo.2022.105038

Gao L, Gao F, Zhang ZZ, Xing Y (2020) Research on the energy evolution characteristics and the failure intensity of rocks. Int J Mining Sci Technol 30:705–713. https://doi.org/10.1016/j.ijmst.2020.06.006

Hallbauer DK, Wagner H, Cook NGW (1973) Some observations concerning the microscopic and mechanical behaviour of quartzite specimens in stiff, triaxial compression tests. Rock Mech 10:713–726. https://doi.org/10.1016/0148-9062(73)90015-6

Hoagland RG, Hahn GT, Rosenfield AR (1973) Influence of microstructure on fracture propagation in rock. Rock Mech 5:77–106. https://doi.org/10.1007/BF01240160

Huan L (2017) Aging rupture mechanism and mesoscopic evolution mechanism of deep heterogeneous rock mass. PhD Thesis, Changjiang River Scientific Research Institute, Wuhan, China (in Chinese)

Jeong SS, Nakamura K, Yoshioka S, Obara Y, Kataoka M (2017) Fracture toughness of granite measured using micro to macro scale specimens. Proced Eng. https://doi.org/10.1016/j.proeng.2017.05.242

Li S, Li D, Wu L, Cao L (2014) Meso-simulation and fractal characteristics for uniaxial compression test of

inhomogeneous rock. J China Coal Soc 39(5):849–854. https://doi.org/10.13225/j.cnki.jccs.2013.0673

Li Q, Li JP, Duan LC, Tan SC (2021) Prediction of rock abrasivity and hardness from mineral composition. Int J Rock Mech Min Sci 140:1–13. https://doi.org/10.1016/j.ijrmms.2021.104658

Li G, Bodahi F, He T, Luo F, Duan S, Li M (2022) Sensitivity analysis of macroscopic mechanical behavior to microscopic parameters based on PFC simulation. Geotech Geol Eng 40:3633–3641. https://doi.org/10.1007/s10706-022-02118-5

Li Y, Chen Y, Gao T, Jing Y, Ma Y (2022) Research on the law of crack propagation and energy dissipation in jointed rock mass. J Shandong Jianzhu Univ 37(2):41–48. https://doi.org/10.12077/sdjz.2022.02.007

Li G, Sun QH, Ma FS, Guo J, Zhao HJ, Wu YF (2023) Damage evolution mechanism and deformation failure properties of a roadway in deep inclined rock strata. Eng Fail Anal 143:1–16. https://doi.org/10.1016/j.engfailanal.2022.106820

Lindqvist JE, Akesson U, Malaga K (2007) Microstructure and functional properties of rock materials. Mater Charact 58:1183–1188. https://doi.org/10.1016/j.matchar.2007.04.012

Quan JS, Rong GA, Xu LD, Chen ZH (2023) A three-dimensional grain-based model for studying the microscopic fracture behaviour of granite. Comput Geotech 159:1–18. https://doi.org/10.1016/j.compgeo.2023.105427

Reches Z, Wetzler N (2022) An energy-based theory of rock faulting. Earth Planet Sci Lett 597:1–9. https://doi.org/10.1016/j.epsl.2022.117818

Rubo RA, Carneiro CD, Michelon MF, Gioria RD (2019) Digital petrography: mineralogy and porosity identification using machine learning algorithms in petrographic thin section images. J Pet Sci Eng 183:1–14. https://doi.org/10.1016/j.petrol.2019.106382

Sun C, Ao Y-h, Zhang J-m, Wang S (2020) Particle flow of meso-fracture characteristics and macro-scale effect of granites. Chin J Geotech Eng 42(9):1687–1695. https://doi.org/10.11779/CJGE202009013

Wang M, Xu T, Deng S, Chen H (2018) Mechanical problems for the long-term stability of rocks surrounding deep level underground tunnels. Explos Shock Waves 41(7):1–15. https://doi.org/10.11883/bzycj-2021-0023

Xie HP, Ju Y, Li LY, Peng RD (2008) Energy mechanism of deformation and failure of rock masses. Chin J Rock Mech Eng 27(9):1729–1740

Yingquan G, Duofeng C, Yue Li, Da H (2022) Mechanism of crack propagation, coalescence and energy evolution of rock mass under unloading condition. Chin J Undergr Space Eng 18(5):1521–1531

Yu H, Liu S, Jia H, Wang S (2020) Mechanical response and energy dissipation mechanism of closed single fractured sandstone under different confining pressures. J Min Saf Eng 37(2):385–393. https://doi.org/10.13545/j.cnki.jmse.2020.02.019

Yu H, Taleghani AD, Lian ZH (2021) A new look at rock mechanical behavior from the meso-scale grain. J Pet Sci Eng 200:1–12. https://doi.org/10.1016/j.petrol.2021.108373

Zhang Y, Miao S-J, Guo Q-F, Wang P-T (2019) Meso-energy evolution and rock burst proneness of the stress thresholds of granite under triaxial cyclic loading and unloading test. Chin J Eng 41(7):864–873. https://doi.org/10.13374/j.issn2095-9389.2019.07.004

Zheng Z, Tang H, Zhang Q, Pan PZ, Zhang XW, Mei GX, Liu ZB, Wang W (2023) True triaxial test and PFC3D-GBM simulation study on mechanical properties and fracture evolution mechanisms of rock under high stresses. Comput Geotech 154:1–24. https://doi.org/10.1016/j.compgeo.2022.105136

Zhu H, Yan J, Liang W (2019) Challenges and development prospects of ultralong and ultra-deep mountain tunnels. Engineering 5(3):384–392. https://doi.org/10.1016/j.eng.2019.04.009